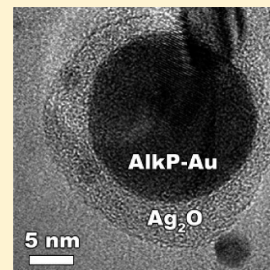# Stabilization of Alkaline Phosphatase with Au@Ag$_2$O Nanoparticles

Brian A. Zaccheo and Richard M. Crooks*

Department of Chemistry and Biochemistry, Texas Materials Institute, and Center for Nano- and Molecular Science and Technology, The University of Texas at Austin, 1 University Station, A5300, Austin, Texas 78712-0165, United States

S *Supporting Information*

ABSTRACT: Here, we report that a conductive Au@Ag$_2$O nanoparticle structure significantly enhances the stability of alkaline phosphatase (AlkP) in the presence of the inhibitors urea and L-phenylalanine (Phe). The enzyme/nanoparticle construct is prepared by associating the enzyme with citrate-capped Au particles, and then adding Ag$^+$. UV−vis and XPS spectroscopy and transmission electron microscopy confirm the core@shell structure. AlkP activity was quantified in the presence and absence of the two inhibitors using a time-resolved colorimetric assay. The results indicate that 21% of the initial active AlkP is incorporated into the nanoparticle structure. More importantly, however, the Au@Ag$_2$O core@shell host reduces the inhibitory effect of urea and Phe by factors ranging from 3 to 12, depending on the inhibitor and its concentration, compared to the wild-type enzyme.

■ INTRODUCTION

Here, we report that alkaline phosphatase (AlkP) is stabilized against organic inhibitors by core@shell colloidal nanoparticles (NPs). These composites are prepared by combining AlkP and an Au colloid solution with Ag$^+$. This results in agglomerated particles having an Ag$_2$O shell (AlkP-Au@Ag$_2$O), which stabilizes and protects the enzyme against inhibitors that would otherwise greatly reduce its activity. This finding is significant, because many applications are carried out under less-than-optimal conditions for enzyme functionality.

AlkP is a common enzyme that has previously been isolated and characterized.[1,2] The wild type (WT) bovine intestinal isoform is an effective catalyst for the hydrolysis of phosphate groups present on a wide variety of substrates, has an approximate molecular weight of 60 kDa, and exhibits optimal activity under moderately basic conditions (pH 9−10).[2] AlkP is often integrated into analytical assays and sensing schemes owing to its ease of handling and high catalytic activity.[1,3] To improve the stability of AlkP and other enzymes used for applications like biosensing, there has been interest in encapsulating them within more rugged host materials. For example, Braun et al. encapsulated AlkP in a bulk sol−gel matrix that was subsequently pulverized and used as column packing material.[4] AlkP in this matrix exhibited a 15% greater tolerance for incubation at 70 °C relative to free AlkP in solution. Smith et al. examined the activity of horseradish peroxidase (HRP) in sol−gel monoliths, coatings, and pulverized powders and reported that the powder form of HRP was active and reusable.[5] These results are also important as they show sol−gel protein entrapment is not exclusive to AlkP. Sol−gels have also been used to protect proteins against drying. For example, Li et al. entrapped a fluorescent protein inside a sol−gel slab and reported that the protein remained fluorescent after lyophilization and rehydration.[6] A loss of the fluorescence signal would indicate changes in the protein structure. The key point common to all of these examples is that sol−gel hosts have been shown to stabilize some proteins against common degradative practices including heating, aging, and drying.

The previously discussed sol−gel materials entrap enzymes within a network of pores.[4] Alternatively, individual enzymes can be stabilized by other types of coatings that are directly attached to the enzyme. For example, Kim et al. modified surface amines on chymotrypsin with alkyl silanols to yield porous silicate gels around the enzyme.[7] This treatment was shown to extend the active lifetime of the enzyme in solution. Thiol groups were used in a similar way to reduce Au^{3+} onto α-amylase and form ∼30 nm NPs that retained amylase activity. Like sol−gels, the Au shell was determined to be porous by screening for amylase activity using substrates with different molecular weights. HRP has been isolated within porous, hollow nanoshells.[8] In this experiment, AgCl-entrapped HRP colloid was prepared inside reverse micelles. HAuCl$_4$ and a reducing agent were phase-partitioned sequentially into the micelles, and after purification of the particles, the AgCl was removed with ammonia to leave active HRP inside an Au shell. Ben-Knaz and Avnir reported that acid phosphatase could be stabilized inside a metal powder by incubating the enzyme in solutions of Ag$^+$ or Au^{3+} and adding Zn^0 as a reducing agent.[9]

In the present manuscript, we report the stabilization of AlkP against the inhibitory chemicals urea and L-phenylalanine (Phe) using composite NPs. We characterized these AlkP-Au@Ag$_2$O NPs using transmission electron microscopy (TEM), UV−vis spectroscopy, X-ray photoelectron spectroscopy (XPS), and energy dispersive spectroscopy (EDS). The results indicate that

AlkP strongly associates with Au colloids and that the addition of Ag^+ to the enzyme-NP conjugate yields a Ag_2O shell. AlkP activity was quantified using a time-resolved colorimetric assay, and the data indicate that ∼21% of the active enzyme initially present is associated with the AlkP-Au@Ag$_2$O composite. Finally, the activity of free AlkP was compared to that of AlkP-Au@Ag$_2$O in the presence of two inhibitors. Under otherwise identical conditions, AlkP-Au@Ag$_2$O was at least three times more active, which demonstrates the stabilizing effect of the Ag_2O shell. Two key advantages of the method described here, compared to previous literature reports, are that this approach uses a one-pot synthesis and the time required to stabilize the enzyme is less than one day.

■ EXPERIMENTAL SECTION

Chemicals and Materials. Citrate-capped Au colloids with a nominal diameter of 5 nm, Silver Enhancer Solution A (henceforth referred to as Ag^+ solution); p-nitrophenol phosphate disodium salt hexahydrate, enzymology grade (pNPP); and L-phenylalanine (Phe), USP, were purchased from Sigma (St. Louis, MO). Calf intestinal AlkP solution was purchased from New England Biolabs, Inc. (Ipswich, MA). Urea, ACS grade, was purchased from Thermo Fisher Scientific (Waltham, MA). Diethanolamine, 99%, was obtained from Alfa Aesar (Ward Hill, MA). Amicon Ultra-4 centrifugal filter sets having a 100 kDa molecular weight cut off (MWCO) were obtained from Millipore (Billerica, MA). Carbon-coated Cu TEM grids, 400 mesh, were purchased from Electron Microscopy Sciences (Hatfield, PA). Disposable UV-transmissive cuvettes with a 1.0 cm path length were purchased from BRAND GmbH (Wertheim, Germany). All chemicals were used as received. Aqueous solutions were prepared using 18 MΩ·cm Milli-Q water (Millipore).

Synthesis of AlkP and NP Solutions. These solutions were prepared using a 1.0 M glycine solution adjusted to pH 9.2. Solutions were prepared in capped glass vials at an ambient temperature of 21 ± 2 °C. Four species were characterized in this work, and they are identified using the following notations: AlkP, Au@Ag$_2$O, AlkP-Au, and AlkP-Au@Ag$_2$O. AlkP solutions of enzyme alone were prepared by combining 4.0 μL of AlkP with 1.35 mL of the glycine solution, and then stirring for ∼18 h. Au@Ag$_2$O, which is a NP species having a Au core and a Ag$_2$O shell (but no enzyme), was prepared by combining 1.0 mL of Au colloid solution and 0.35 mL of glycine, stirring for ∼18 h, and then adding 50.0 μL of Ag^+ solution. The mixture was then stirred for an additional 2.0 h. AlkP-Au, which is an enzyme-Au colloid conjugate, was prepared by combining 1.0 mL of Au colloid solution, 0.35 mL of glycine, 4.0 μL of AlkP, and then stirring for ∼18 h. AlkP-Au@Ag$_2$O was prepared as described for AlkP-Au, with the additional steps of adding 50.0 μL of Ag^+ solution followed by stirring for 2.0 h. All species were isolated by filtration in which the crude solution was transferred to the reservoir of a MWCO tube and centrifuged for 10.0 min at 3000g. The filtrate was collected, and the pellet was resuspended with 1.0 mL of water and centrifuged again for 10.0 min at 3000g. The eluted liquid, hereafter referred to as the wash, was pooled with the initial filtrate and retained for analysis. The pellet was resuspended with 1.0 mL of water and transferred to a microcentrifuge tube for subsequent analysis.

Characterization. UV−vis spectra of filtered and desalted solutions of Au colloid, Au@Ag$_2$O, AlkP-Au, and AlkP-Au@Ag$_2$O were obtained using a Hewlett-Packard HP8453 spectrometer (Santa Clara, CA). TEM micrographs of AlkP-Au, Au@Ag$_2$O, and AlkP-Au@Ag$_2$O were collected on a FEI TECNAI G2 F20 X-TWIN instrument (Hillsboro, OR). Grids were prepared by drop-casting 5.0 μL of each solution onto a TEM grid and drying overnight in a vacuum desiccator.

Element maps and scanning/transmission electron microscope (STEM) images of AlkP-Au@Ag$_2$O were captured on a Hitachi S5500 with a Bruker Quantax 4010 EDS detector operating at 30 kV in bright-field mode (Pleasanton, CA, and Billerica, MA, respectively). TEM grids for STEM and EDS were prepared as for TEM, but included an extra drying step where the grids were lyophilized for 48 h. XPS analysis was carried out using a Kratos Axis Ultra spectrometer having an Al Kα filament (Chestnut Ridge, NY). XPS spectra were collected for Au colloid, Au@Ag$_2$O, AlkP-Au, AlkP-Au@Ag$_2$O, and WT AlkP. Samples of Au colloid, Au@Ag$_2$O, AlkP-Au, and AlkP-Au@Ag$_2$O were prepared by drop-casting 20 μL volumes onto sections of Si wafer and drying for 24 h in a vacuum desiccator. WT AlkP specimens were prepared by drop-casting 10 μL of AlkP solution onto Au-coated glass and drying for 24 h in a vacuum desiccator. Spectra were collected at a pass energy of 20 eV with a step size of 0.1 eV for individual element scans. Sample charging was compensated by referencing the observed C 1s C−C peak to 284.5 eV.[10]

AlkP Activity Assay. Time-resolved colorimetric assays were used to measure the active quantity of AlkP in diethanolamine (DEA) units (U) for WT AlkP, AlkP-Au, Au@Ag$_2$O, and AlkP-Au@Ag$_2$O. One AlkP DEA U is defined as the amount of enzyme required to hydrolyze 1 μmol of pNPP per minute. Activity testing was performed for each sample on the pooled filtrate and wash fraction, and on the resuspended pellet fraction. The activity assay method was adapted from literature reports.[11,12] Assays were carried out in a buffer containing 1.0 M DEA and 1.0 mM MgSO$_4$ adjusted to pH 9.8 with H$_2$SO$_4$. Briefly, 1.7 mL of buffer, 20.0 μL of the test solution, and 0.10 mL of 150 mM pNPP were added to a cuvette and mixed by repetitive pipetting. The absorbance at 405 nm (A_{405}) was recorded at 0.50 min intervals for 6.0 min. A least-squares fit was applied to the linear data to obtain the change in A_{405} as a function of time (ΔA_{405} min^{-1}). The activity in U was then calculated from the ΔA_{405} min^{-1} value as described in the literature.[11] Between 3 and 5 replicates for each analyte were assayed.

Inhibition assays were performed on solutions of WT AlkP, AlkP-Au, and AlkP-Au@Ag$_2$O. For these assays, either urea or Phe was added to the DEA solution prior to testing. AlkP activity was measured at urea concentrations of 2.5 or 5.0 M and Phe concentrations of 10.0 or 50.0 mM; the UV−vis blank contained DEA buffer, inhibitor at an appropriate concentration, and pNPP. The inhibitor assays were performed using the same procedure as the activity assays, with the added step of allowing the test solution and inhibitor-containing DEA solution to incubate for 30.0 min prior to pNPP addition and UV−vis analysis. Different concentrations of enzyme were necessarily used for the WT AlkP, AlkP-Au, and AlkP-Au@Ag$_2$O assays, and therefore, the results were normalized as discussed in the Supporting Information.

■ RESULTS AND DISCUSSION

As discussed in detail in the Experimental Section, AlkP-Au@Ag$_2$O colloids were prepared in three steps. First, AlkP was mixed with citrate-capped Au colloid and glycine solutions. Glycine is compatible with AlkP activity[2] without adversely affecting the Au colloids.[13] Second, a Ag^+ solution was added to this mixture. After incubation, the resulting material was purified and characterized. Additional information about the synthesis of the other NP species discussed in this report is provided in the Experimental Section.

TEM micrographs of Au@Ag$_2$O and AlkP-Au@Ag$_2$O are shown in Figure 1. In Figure 1a, two populations of Au@Ag$_2$O particles are evident: discrete particles and small aggregates. The core@shell nature of these materials is suggested by the contrast difference between the dark centers and lighter periphery. The contrast difference is more apparent in the higher magnification image provided in the inset. In Figure 1b, two populations of
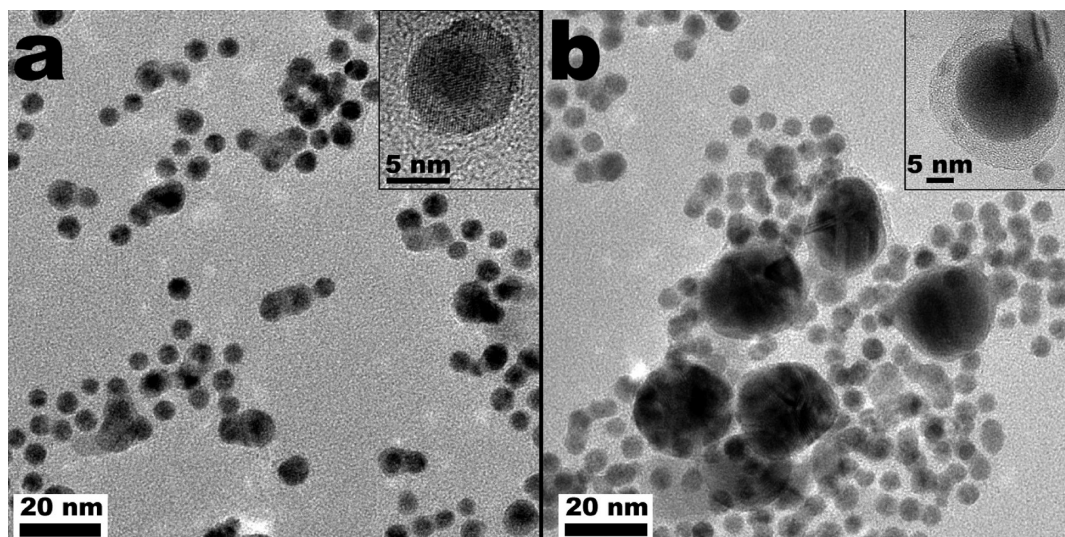
Figure 1. TEM micrographs of (a) Au@Ag$_2$O and (b) AlkP-Au@Ag$_2$O. Two particle populations are present for each species. The insets show higher magnification images of individual particles and highlight the core@shell morphology.
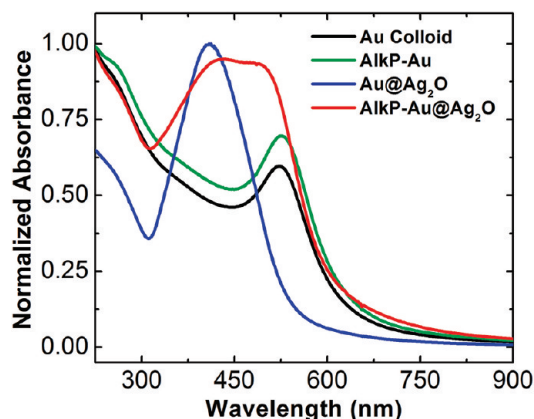

Figure 2. UV–vis spectra of desalted, aqueous solutions of Au colloids, AlkP-Au, Au@Ag$_2$O, and AlkP-Au@Ag$_2$O. The absorbance has been normalized to facilitate comparison of the spectra.

AlkP-Au@Ag$_2$O are also observed: small spherical particles and larger agglomerates. The smaller particles resemble the Au@Ag$_2$O NPs in Frame a. The larger clusters were observed consistently in AlkP-Au@Ag$_2$O preparations, but they were not present in Au@Ag$_2$O samples. The inset of Figure 1b shows a high magnification image of a large AlkP-Au@Ag$_2$O agglomerate, and it is apparent that these materials also have a core@shell structure. TEM analysis of AlkP-Au (Supporting Information, Figure S1) indicates well-dispersed, unagglomerated particles exhibiting uniform contrast. On the basis of the morphology of the large AlkP-Au@Ag$_2$O agglomerates and their presence only in the AlkP-Au@Ag$_2$O images, we draw two conclusions. First, the large AlkP-Au@Ag$_2$O agglomerates have a core@shell structure. Second, the formation of large agglomerates depends on the presence of AlkP.

UV–vis spectra for desalted, aqueous solutions of Au colloids, Au@Ag$_2$O, AlkP-Au, and AlkP-Au@Ag$_2$O are shown in Figure 2. Each spectrum was normalized to a maximum absorbance of 1.0 to facilitate comparison of the spectra. The Au colloid starting material has a peak centered at 523 nm, which corresponds to the

plasmon reported for Au NPs in this size range.[14] The solution containing AlkP-Au is similar to that of the Au colloid solution except for a slight shift in the plasmon band to 527 nm.

The spectrum of Au@Ag$_2$O reveals the effect of Ag deposition onto the Au colloids. In this case, a new peak is observed at 410 nm, but the Au plasmon previously observed in the spectra of the Au colloid and AlkP-Au solutions is absent. The position of the new peak arising from Au@Ag$_2$O corresponds to a Ag plasmon, which has previously been reported in the literature for Ag colloids, Ag$_2$O thin films, and Ag NPs having a Ag$_2$O shell (Ag@Ag$_2$O).[15−17] The position of the peak observed for Au@Ag$_2$O is also similar to the plasmon band reported for bimetallic Au@Ag nanoparticles, in which the Au plasmon is quenched by the presence of the Ag (or Ag$_2$O) shell.[18,19] Accordingly, this finding is consistent with the core@shell structure revealed by the TEM images in Figure 1a.

The spectrum of AlkP-Au@Ag$_2$O is different than the other three spectra in that it exhibits two overlapping peaks at 427 and 505 nm. The position of the 427 nm peak is consistent with Ag$_2$O. However, the presence of the peak at 505 nm suggests that some fraction of the Au surface, probably in the larger agglomerates (Figure 1b), is not covered with Ag$_2$O. This view is consistent with results reported by Gonzalez et al., who observed a similar spectrum for bimetallic Au@Ag nanoparticles having only a partial Ag shell.[18] Because protein adhesion to Au NPs is well documented,[20] we speculate that AlkP is responsible for incomplete Ag$_2$O coverage and hence the band at 505 nm.

XPS Analysis. XPS spectra collected for Au colloids, Au@Ag$_2$O, AlkP-Au@Ag$_2$O, and WT AlkP are provided in Figure 3.[21] The high-resolution C spectra in Figure 3a exhibit binding energies consistent with those reported for C–C, C–N, and C–O bonds.[10] For example, the C 1s spectrum for Au@Ag$_2$O consists of two peaks having binding energies corresponding to C–C and C–O bonds.[10] The presence of a C–O peak can be attributed to the citrate capping agent on the Au colloids. The spectrum of AlkP-Au@Ag$_2$O exhibits three dominant features. Two of these peaks have energies coincident with the C–C and C–O bonds in the Au@Ag$_2$O spectrum. The binding energy of the center peak in the AlkP-Au@Ag$_2$O spectrum is suggestive of
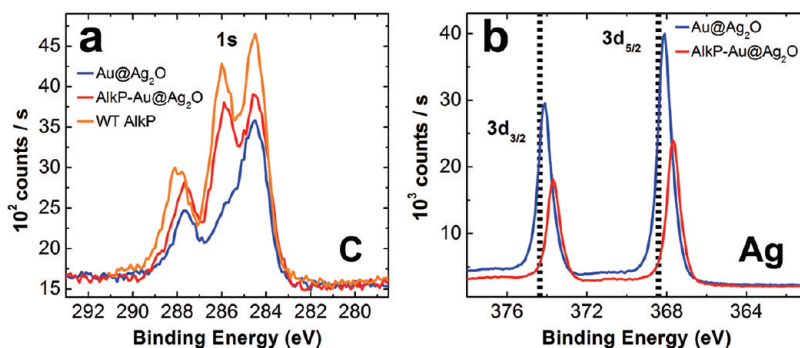
Figure 3. (a) High-resolution C 1s XPS spectra for Au@Ag$_2$O, AlkP-Au@Ag$_2$O, and WT AlkP. The three features correspond to C—C (284.5 eV), C—N (286.0 eV), and C—O (287.5 eV) functional groups. (b) Ag 3d XPS spectra for Au@Ag$_2$O and AlkP-Au@Ag$_2$O. The dashed lines represent the 3d$_{5/2}$ and 3d$_{3/2}$ reference energies for Ag^0.
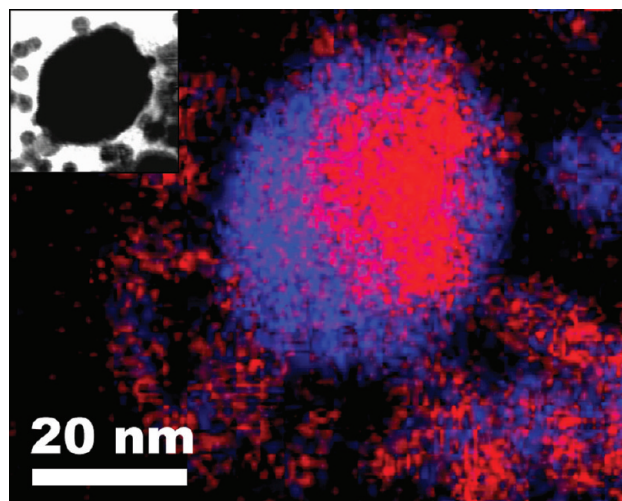

Figure 4. EDS element map of a AlkP-Au@Ag$_2$O agglomerate and smaller, nearby Au@Ag$_2$O particles. The image is rendered in false color: Ag is shown in blue and Au in red. The inset is an STEM image of the EDS field-of-view.

C—N bonding. These three features also appear in WT AlkP. Recalling that the AlkP-Au@Ag$_2$O solution was washed and filtered to remove free enzyme prior to XPS analysis, we conclude that AlkP is entrapped within these Au@Ag$_2$O agglomerates.

The high-resolution Ag 3d XPS spectra of Au@Ag$_2$O and AlkP-Au@Ag$_2$O are provided in Figure 3b. Dashed lines indicate the reported binding energies for zerovalent Ag (368.3 and 374.3 eV).[10,22] The 3d$_{5/2}$ peaks for Au@Ag$_2$O and AlkP-Au@Ag$_2$O appear at 368.1 and 367.7 eV, respectively, which are somewhat lower than the corresponding literature value for zerovalent Ag.[10] However, these binding energies are consistent with values reported for Ag$_2$O (between 367.5 and 368.2 eV).[10,15,23] That Ag$_2$O has a more negative binding energy than zerovalent Ag is attributed to the electronic structure of Ag$_2$O and its metal-like conductivity.[24,25] We conclude that Ag$_2$O is the principal Ag species present in both Au@Ag$_2$O and AlkP-Au@Ag$_2$O. Ag$_2$O may form via reduction of Ag$^+$ to Ag^0 by citrate,[26] which is used to stabilize the Au colloids, followed by reaction with oxygen to yield Ag$_2$O. High-resolution XPS spectra in the Au region are provided in Supporting Information Figure S2 and indicate the presence of zerovalent Au only.

EDS Mapping. We used element mapping to carry out spatially resolved analysis of the large AlkP-Au@Ag$_2$O agglomerates shown in Figure 1b. Figure 4 is a drift-corrected element map, rendered in false color, of a single cluster surrounded by several smaller particles. The inset is an STEM image of the EDS field of view. The map reveals two interesting features. First, the elemental distribution in the large cluster is consistent with that of a Au@Ag$_2$O core@shell morphology. Second, its Au core is much larger than the ~5 nm colloids, which were the initial source of Au. This indicates the presence of multiple Au colloids in the core.

Activity Assays and Inhibition. Colorimetric activity assays were used to quantify the amount of AlkP present during each step of the synthesis of AlkP-Au@Ag$_2$O. The DEA assay described in the Experimental Section was selected to determine the AlkP concentration in activity units, because it reports an absolute quantity of the functional enzyme. As discussed earlier, the metal-containing solutions were purified to ensure that free AlkP was removed. This step is important for interpreting the activity assay, because it ensures that the measured activity arises only from AlkP associated with agglomerates. Filtration and washing steps were used for purification, and they result in three fractions. The initial filtrate consists of unbound AlkP, solvent, glycine, and salts that were introduced during the synthesis. The wash solution was used to ensure removal of free AlkP from the retained solid material comprises the second fraction. Finally, the solid remaining after the wash step was taken up in water, and this represents the third fraction. The filtrate and wash fractions were pooled and analyzed for enzyme activity alongside the resuspended solid for each of the following samples: WT AlkP, Au@Ag$_2$O, AlkP-Au, and AlkP-Au@Ag$_2$O. Information about the analysis of these data is provided in the Experimental Section.

The results from the activity assays, in terms of catalytically active enzyme units (U), are presented in Table 1. For WT AlkP, we find that essentially all enzyme activity arises from the pooled filtrate and wash, which is consistent with expectations for filtration of a 60 kDa molecular weight enzyme through a 100 kDa MWCO filter. Also consistent with expectations, the enzyme-free Au@Ag$_2$O particles registered effectively zero activity.

The effect of NPs on the activity of the enzyme is revealed by the results of the AlkP-Au assay. Here, there is a decrease in the total enzyme activity compared to free WT AlkP, which is typical for enzymes adsorbed to metal surfaces.[27] Specifically, the total enzyme activity for the AlkP-Au material (pellet, filtrate, and

Table 1. Active Quantity of AlkP in DEA Units (U) for the WT AlkP, Au@Ag₂O, AlkP-Au, and AlkP-Au@Ag₂O Species by Fraction[a]

species	filtrate + wash activity (U)	pellet activity (U)	total activity (U)
WT AlkP	1.65 ± 0.07	0.022 ± 0.003	1.67 ± 0.07
Au@Ag₂O	0 ± 0.005	0.030 ± 0.046	0.030 ± 0.05
AlkP-Au	0.49 ± 0.07	0.87 ± 0.11	1.37 ± 0.13
AlkP-Au@Ag₂O	0.79 ± 0.05	0.21 ± 0.01	1.00 ± 0.05

[a] Activities were measured for the pooled filtrate plus wash fractions and the resuspended pellet. The total activity is shown in the column on the right. The values shown represent the average of 3−5 replicates carried out using independently prepared materials ($\pm 1\sigma$).
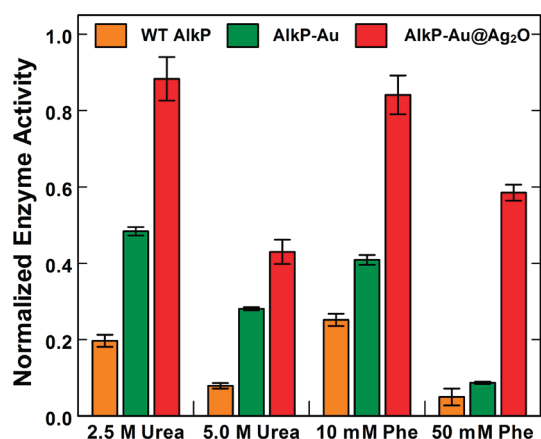

Figure 5. Histogram comparing inhibition data for WT AlkP, AlkP-Au, and AlkP-Au@Ag₂O in the presence of 2.5 and 5.0 M urea, and 10.0 and 50.0 mM Phe. Error bars represent $\pm 1\sigma$ from the mean. An explanation of how the normalized enzyme activity was calculated is provided in the Supporting Information.

wash; Table 1) is ∼82% that of the total free WT enzyme. Analysis of AlkP-Au@Ag₂O fractions indicates that the majority of the enzyme is eluted in the filtrate and wash. In fact, somewhat surprisingly, there is more free enzyme observed with AlkP-Au@Ag₂O than with AlkP-Au. This could be due to displacement of AlkP from the Au surface during formation of the Ag₂O shell. Finally, we find that 13% of the AlkP activity is retained in AlkP-Au@Ag₂O pellet compared to the total free WT AlkP. This is not a high degree of activity, but as we will see in the next section, the 13% remaining is quite stable in the presence of inhibitors.

Inhibition Assays. The activities of WT AlkP, AlkP-Au, and AlkP-Au@Ag₂O were quantified in the presence of inhibitors to evaluate the stabilizing effect of the Ag₂O shell. The inhibition assays were performed in the same manner as the activity assay described in the previous section, except for the presence of the inhibitors urea or Phe. Urea is a denaturant that disrupts the secondary structure of AlkP.[1] Phe is an uncompetitive inhibitor that delays the release of product from AlkP.[28,29]

The normalized activities of AlkP, AlkP-Au, and AlkP-Au@Ag₂O in the presence of two different concentrations of urea and Phe are compared in Figure 5. Different concentrations of enzyme were used for the WT AlkP, AlkP-Au, and AlkP-Au@Ag₂O assays, and therefore, the results were normalized as

discussed in the Supporting Information. WT AlkP was strongly inhibited in this assay, and exhibited a normalized activity of <0.30 for urea and Phe at both concentrations. The normalized activity of AlkP-Au was found to be <0.50 in all cases. These data indicate that the surface adsorption of AlkP onto Au colloids in AlkP-Au provides some protective benefit. However, a more notable enhancement in activity is observed for the enzyme in the form of AlkP-Au@Ag₂O. Indeed, AlkP-Au@Ag₂O remained almost fully active in the presence of the dilute inhibitors, and even at the high inhibitor concentrations AlkP-Au@Ag₂O was more active than either WT AlkP or AlkP-Au. We conclude that the Ag₂O shell provides a significant degree of stability for AlkP in the presence of urea and Phe, while still providing access to the substrate used for the assay. Although we have only examined urea and Phe, it seems likely the approach described here will extend to other inhibitors.

■ SUMMARY AND CONCLUSIONS

We have described a means for stabilizing AlkP against two inhibitors: urea and Phe, which operate on the enzyme by different mechanisms. Structural characterization suggests that the enzyme is incorporated into a conductive Au@Ag₂O core@-shell structure, but beyond this, we are not prepared to discuss the molecular-level details that lead to stabilization. There are two aspects of the findings reported here that are significant. First, the stabilizing agent is electrically conductive, and therefore there is a chance that this approach, or one like it, could be used to stabilize redox enzymes and electrically wire them to an electrode surface. Second, the time required to prepare the AlkP-Au@Ag₂O construct is one day. This is significantly faster than has been reported previously for sol−gel and other types of enzyme stabilizers.[4,5,8]

■ ASSOCIATED CONTENT

Ⓢ Supporting Information. TEM micrographs of AlkP-Au, Au 4f XPS spectra, and an explanation of how the results presented in Figure 5 were calculated. This material is available free of charge via the Internet at http://pubs.acs.org.

■ AUTHOR INFORMATION

Corresponding Author
*E-mail: crooks@cm.utexas.edu; Voice: 512-475-8674.

■ ACKNOWLEDGMENT

■ REFERENCES

(1) Simopoulos, T. T.; Jencks, W. P. Alkaline Phosphatase Is an Almost Perfect Enzyme. *Biochemistry* **1994**, *33*, 10375−10380.

(2) Morton, R. K. Some properties of alkaline phosphatase of cow's milk and calf intestinal mucosa. *Biochem. J.* **1955**, *60*, 573−582.

(3) Zaccheo, B. A.; Crooks, R. M. Detection of an Epstein—Barr Genome Analog at Physiological Concentrations via the Biometallization of Interdigitated Array Electrodes. *Anal. Chem.* **2009**, *81*, 5757–5761.

(4) Braun, S.; Rappoport, S.; Zusman, R.; Avnir, D.; Ottolenghi, M. Biochemically Active Sol-Gel Glasses - the Trapping of Enzymes. *Mater. Lett.* **1990**, *10*, 1–5.

(5) Smith, K.; Silvernail, N. J.; Rodgers, K. R.; Elgren, T. E.; Castro, M.; Parker, R. M. Sol—Gel Encapsulated Horseradish Peroxidase: A Catalytic Material for Peroxidation. *J. Am. Chem. Soc.* **2002**, *124*, 4247–4252.

(6) Li, Y. K.; Chou, M. J.; Wu, T. Y.; Jinn, T. R.; Chen-Yang, Y. W. A Novel method for preparing a protein-encapsulated bioaerogel: Using a red fluorescent protein as a model. *Acta Biomater.* **2008**, *4*, 725–732.

(7) Kim, J.; Grate, J. W. Single-Enzyme Nanoparticles Armored by a Nanometer-Scale Organic/Inorganic Network. *Nano Lett.* **2003**, *3*, 1219–1222.

(8) Kumar, R.; Maitra, A. N.; Patanjali, P. K.; Sharma, P. Hollow gold nanoparticles encapsulating horseradish peroxidase. *Biomaterials* **2005**, *26*, 6743–6753.

(9) Ben-Knaz, R.; Avnir, D. Bioactive enzyme-metal composites: The entrapment of acid phosphatase within gold and silver. *Biomaterials* **2009**, *30*, 1263–1267.

(10) Moulder, J. F.; Bomben, K. D.; Sobol, P. E.; Stickle, W. F. *Handbook of X-ray Photoelectron Spectroscopy*; Physical Electronics USA, Inc: Chigasaki, Japan, 1995.

(11) Enzymatic Assay of PHOSPHATASE, ALKALINE. January 20, 2011; http://www.sigmaaldrich.com/etc/medialib/docs/Sigma/Enzyme_Assay/phosphalkeieth.Par.0001.File.dat/phosphalkeieth.pdf.

(12) Walter, K.; Schuett, C. in *Methods of Enzymatic Analysis*, Bergmeyer, H. U., Ed.; Academic Press, Inc.: New York, 1974; pp 860—864.

(13) Hamaguchi, K.; Kawasaki, H.; Arakawa, R. Photochemical synthesis of glycine-stabilized gold nanoparticles and its heavy-metal-induced aggregation behavior. *Colloids Surf., A* **2010**, *367*, 167–173.

(14) Perrault, S. D.; Chan, W. C. W. Synthesis and Surface Modification of Highly Monodispersed, Spherical Gold Nanoparticles of 50—200 nm. *J. Am. Chem. Soc.* **2009**, *131*, 17042–17043.

(15) Chiu, Y.; Rambabu, U.; Hsu, M. H.; Shieh, H. P. D.; Chen, C. Y.; Lin, H. H. Fabrication and nonlinear optical properties of nanoparticle silver oxide films. *J. Appl. Phys.* **2003**, *94*, 1996–2001.

(16) Schinca, D. C.; Scaffardi, L. B.; Videla, F. A.; Torchia, G. A.; Moreno, P.; Roso, L. Silver-silver oxide core-shell nanoparticles by femtosecond laser ablation: core and shell sizing by extinction spectroscopy. *J. Phys. D.* **2009**, *42*, 215102–215111.

(17) Soukupova, J.; Kvitek, L.; Kratochvilova, M.; Panacek, A.; Prucek, R.; Zboril, R. Silver Voyage from Macro- to Nanoworld. *J. Chem. Educ.* **2010**, *87*, 1094–1097.

(18) Gonzalez, C. M.; Liu, Y.; Scaiano, J. C. Photochemical Strategies for the Facile Synthesis of Gold—Silver Alloy and Core—Shell Bimetallic Nanoparticles. *J. Phys. Chem. C* **2009**, *113*, 11861–11867.

(19) Wilson, O. M.; Scott, R. W. J.; Garcia-Martinez, J. C.; Crooks, R. M. Synthesis, Characterization, and Structure-Selective Extraction of 1—3-nm Diameter AuAg Dendrimer-Encapsulated Bimetallic Nanoparticles. *J. Am. Chem. Soc.* **2004**, *127*, 1015–1024.

(20) Zhang, D.; Neumann, O.; Wang, H.; Yuwono, V. M.; Barhoumi, A.; Perham, M.; Hartgerink, J. D.; Wittung-Stafshede, P.; Halas, N. J. Gold Nanoparticles Can Induce the Formation of Protein-based Aggregates at Physiological pH. *Nano Lett.* **2009**, *9*, 666–671.

(21) Heinrich, K. F. J. *Electron Beam X-Ray Microanalysis*; Van Nostrand Reinhold Company: New York, 1981.

(22) Seah, M. P. Post-1989 calibration energies for X-ray photoelectron spectrometers and the 1990 Josephson constant. *Surf. Interface Anal.* **1989**, *14*, 488.

(23) Hammond, J. S.; Gaarenstroom, S. W.; Winograd, N. X-ray photoelectron spectroscopic studies of cadmium- and silver-oxygen surfaces. *Anal. Chem.* **1975**, *47*, 2193–2199.

(24) Deb, A.; Chatterjee, A. K. The electronic structure and chemical bonding mechanism of silver oxide. *J. Phys.: Condens. Matter* **1998**, *10*, 11719–11729.

(25) Raju, N. R. C.; et al. Physical properties of silver oxide thin films by pulsed laser deposition: effect of oxygen pressure during growth. *J. Phys. D* **2009**, *42*, 135411.

(26) Rivas, L.; Sanchez-Cortes, S.; García-Ramos, J. V.; Morcillo, G. Growth of Silver Colloidal Particles Obtained by Citrate Reduction To Increase the Raman Enhancement Factor. *Langmuir* **2001**, *17*, 574–577.

(27) Suckling, C. J. Immobilized enzymes. *Chem. Soc. Rev.* **1977**, *6*, 215–233.

(28) Fernley, H. N.; Walker, P. G. Inhibition of alkaline phosphatase by L-phenylalanine. *Biochem. J.* **1970**, *116*, 543–544.

(29) Ghosh, N. K.; Fishman, W. H. On the Mechanism of Inhibition of Intestinal Alkaline Phosphatase by l-Phenylalanine. *J. Biol. Chem.* **1966**, *241*, 2516–2522.